JACS
JOURNAL OF THE AMERICAN CHEMICAL SOCIETY

Article

pubs.acs.org/JACS

Wave Function Engineering for Efficient Extraction of up to Nineteen Electrons from One CdSe/CdS Quasi-Type II Quantum Dot

Haiming Zhu, Nianhui Song, William Rodríguez-Córdoba, and Tianquan Lian*

Department of Chemistry, Emory University, Atlanta, Georgia 30322, United States

Supporting Information

ABSTRACT: Solar-to-fuel conversion devices require not only efficient catalysts to accelerate the reactions, but also light harvesting and charge separation components to absorb multiple photons and to deliver multiple electrons/holes to the catalytic centers. In this paper, we show that the spatial distribution of electron and hole wave functions in CdSe/CdS quasi-type II quantum dots enables simultaneous ultrafast charge separation (0.18 ps to adsorbed Methylviologen), ultraslow charge recombination (0.4 μs), and slow multiple-exciton Auger annihilation (biexciton lifetime 440 ps). Up to nineteen excitons per QD can be generated by absorbing multiple 400 nm photons and all excitons can be dissociated with unity yield by electron transfer to adsorbed methylviologen molecules. Our finding demonstrates that (quasi-) type II nanoheterostructures can be engineered to efficiently dissociate multiple excitons and deliver multiple electrons to acceptors, suggesting their potential applications as light harvesting and charge separation components in artificial photosynthetic devices.

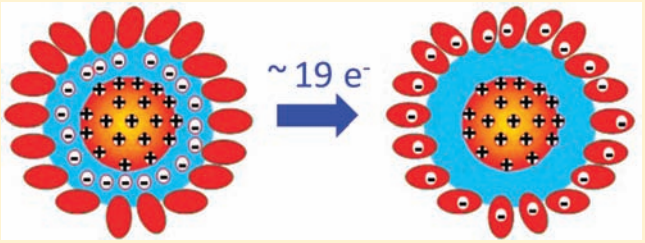

INTRODUCTION

Direct solar-to-fuel conversion is a promising approach for generating renewable clean energy.[1] Many desirable solar fuel forming reactions require multiple reduction and oxidation steps.[2−4] For example, the oxidation of water ($2H_2O \rightarrow O_2 + 4H^+ + 4e^-$) requires the removal of four electrons and the formation of H_2 from protons ($2H^+ + 2e^- \rightarrow H_2$) needs the addition of two electrons. Thus solar-to-fuel conversion devices require not only efficient catalysts to accelerate the reactions, but also a machinery to accumulate multiple electrons/holes needed in the catalytic centers through sequential single photon absorption and single electron transfer events in light harvesting components. In photosynthetic systems in nature, the four oxidative equivalents needed to oxidize water are accumulated by the use of Z-scheme, in which finely tuned protein arrays with specific spatial distributions and energetic gradients enable eight sequential single photon induced long distance single electron transfers while suppressing charge recombination.[5,6] Most molecular chromophores, like the ones used in natural photosynthetic systems, change their absorption properties dramatically upon excitation or redox events, often losing the ability to harvest additional solar photons until returning to its initial state.[7] Due to delocalized electrons and continuous electronic levels in the conduction and valence bands, semiconductor nanomaterials can continue to absorb efficiently after accumulation of electrons and/or holes, a unique property that may provide an alternative approach to construct simpler artificial photosynthetic systems.

Using semiconductor nanocrystals or quantum dots (QDs) as light harvesting and charge separation materials in solar energy conversion devices have been a subject of intense recent interest.[8−11] Semiconductor nanocrystals can generate and accumulate multiple excitons through either direct multiexciton generation (MEG) by one high energy photon or multiple photon absorption (MPA).[12−16] In bulk semiconductors, diffusion of electrons/holes from the interior to the surface attached catalysts can be inefficient because of their limited surface areas and competitive electron−hole recombination processes.[17] In semiconductor QDs and related nanostructures, in addition to the increased catalyst concentration afforded by the large effective surface area (i.e., larger surface area/volume ratio), the confinement of electrons and holes lead to enhanced amplitudes of their wave functions at the surface, enabling direct and efficient dissociation of excitons by interfacial electron or hole transfer to surface adsorbed acceptors or catalysts.[11,18−24] Unfortunately, the small volume of quantum dots also enhances exciton Auger recombination process, wherein an electron−hole pair (exciton) nonradiatively recombines by transferring its energy to a third carrier (Figure 1).[25−27] The Auger recombination occurs on the 10−100 ps time scale for biexcitons in CdSe QDs, and its rate becomes faster with increased number of excitons, competing with the extraction of multiple electrons and holes needed to drive photocatalytic reactions.[26,28] Furthermore, efficient photocatalysis requires not only fast interfacial charge separation but also slow charge recombination (back reaction). In small nanoparticles, both the amplitudes of electron and hole wave functions at the surface are enhanced, speeding up both the initial charge separation and the subsequent charge recombi-

Received: November 2, 2011
Published: February 13, 2012

dx.doi.org/10.1021/ja210312s | J. Am. Chem. Soc. 2012, 134, 4250−4257

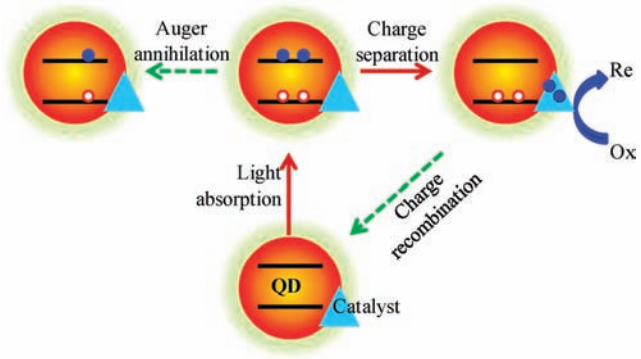

Figure 1. Competition of multiexciton dissociation and catalysis with exciton annihilation and charge recombination processes in quantum dot-catalyst complexes.

nation processes.[20,29] Therefore, in QDs, both the enhanced exciton Auger recombination and interfacial recombination of the separated charges hinder their applications as multi-electron/hole transfer centers in photocatalytic systems (Figure 1).

In colloidal nanoheterostructures (core/shell QDs or nanorods), the relative conduction band (CB) and valence band (VB) positions of the component materials can be chosen to tailor the electron and hole distributions (i.e., wave function engineering) to control the single and multiple exciton lifetimes within the nanostructure as well as to optimize the rate and efficiency of interfacial charge transfer to external acceptors.[30−36] It has been shown that in type II or quasi-type II core/shell QDs, such as CdTe/CdSe and CdSe/CdS QDs, respectively, the spatially separated 1S electron and hole wave functions reduced their Coulomb interaction, increasing the lifetimes of single and multiple exciton states.[31,37−39] Type II core/shell QDs with shell-localized 1S electrons and core-localized 1S holes can achieve ultrafast electron transfer (ET) to adsorbed acceptors while simultaneously retard the charge recombination process.[18,19] The combined properties of long multiexciton lifetimes, efficient charge separation, and slow recombination in (quasi-) type II heterostructures suggest that these may be ideal materials for delivering multiple electrons to catalysts or redox mediators in artificial photosynthetic systems.

In this study, we investigate the capability of CdSe/CdS quasi-type II core/shell QDs for storing multiple excitons and transferring multiple electrons to surface adsorbed methylviologen (MV^{2+}) molecules (a widely used electron acceptor and mediator). We show that compared with CdSe or CdS core only QDs, the delocalized electron wave function in CdSe/CdS QDs maintains ultrafast electron transfer to MV^{2+} whereas the strongly core confined hole wave function greatly slows down the interfacial charge recombination process. The efficient charge separation and lengthened multiexciton lifetime in these materials enables efficient photodriven multiple electron transfer to adsorbed MV^{2+} molecules. As many as nineteen excitons can be generated in one CdSe/CdS QD under 400 nm excitation, and in the presence of adsorbed MV^{2+}, all nineteen excitons can be dissociated by interfacial electron transfer. This result demonstrates the feasibility of using nanoheterostructures as multielectron transferring light harvesting and charge separation materials.

RESULTS AND DISCUSSION

Characterization of CdSe/CdS Quasi-Type II Quantum Dots. The CdSe/CdS core−shell QDs were synthesized following a previously reported successive ion layer adsorption and reaction method (see SI1).[40] We started with a small CdSe core (~1.2 nm radius) and coated it with a CdS shell (~2.2 nm from TEM measurement). According to an effective mass calculation, the details of which can be found in SI3, these particles have a quasi-type II band alignment with a delocalized 1S electron throughout the core and shell and a strongly core-confined 1S hole (Figure 2A). This finding is consistent with

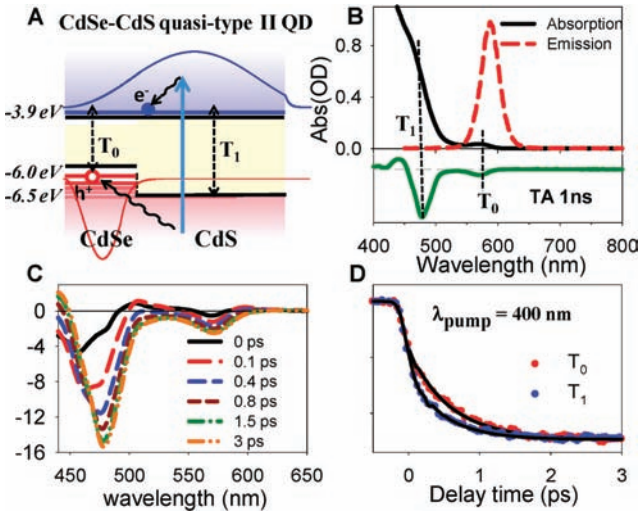

Figure 2. (A) Schematic energy level diagram and lowest energy electron and hole wave functions in CdSe/CdS (core/shell) quasi-type II QDs. According to an effective mass calculation (see SI3), the electron wave function (blue solid line) is delocalized and hole wave function (red solid line) is localized in the core. The black dashed vertical arrows connect the levels involved in the T_0 and T_1 transitions and the curved arrows indicate the electron and hole relaxation processes after 400 nm excitation (blue arrow). (B) Static absorption (black solid line) and static emission (red dashed line) and transient absorption (at 1 ns, green line) spectra of CdSe/CdS QDs. (C) Transient absorption spectra and (D) bleach formation kinetics of T_0 (575 nm) and T_1 (475 nm) bands of CdSe/CdS QDs at indicated delay times (0−3 ps) after 400 nm excitation (at low intensity ~27 $\mu W/cm^2$).

previous experimental studies and calculations of CdSe/CdS core/shell QDs of similar core and shell dimensions.[38,41] As shown in Figure 2B, the static ultraviolet and visible (UV−vis) absorption spectrum exhibits a peak at 575 nm (denoted as T_0) and a much more intense bulk-like continuous absorption band with an onset at ~475 nm (denoted as T_1), which is more clearly seen in the transient absorption (TA) spectrum. The T_0 band is close to the emission peak at 590 nm (Figure 2B) and can be assigned to the transition between the lowest energy CB electron ($1S_e$) and VB hole ($1S_h$) levels in the core/shell structure ($1S_e-1S_h$). As shown in the transient absorption (TA) spectrum at 1 ns (Figure 2B), the formation of 1S exciton state leads to bleaches at both the T_1 and T_0 bands, suggesting that these transitions involve the same $1S_e$ level. Therefore, the T_1 band is assigned to the transition between the delocalized $1S_e$ level and the lowest energy hole level above the VB band edge of the CdS shell. The transitions between the quasi continua of higher energy electron and hole levels give rise to the bulk-like absorption feature seen in Figure 2B. The

dx.doi.org/10.1021/ja210312s | J. Am. Chem. Soc. 2012, 134, 4250−4257

transition energies of the T_1 and T_0 bands are in good agreement with the calculated values (SI3), and the identities of the involved electron and hole levels are consistent with the excitation wavelength dependent carrier dynamics in CdSe/CdS QDs (SI4), providing further support of this assignment.

Single Exciton Charge Separation and Recombination Kinetics in CdSe/CdS QDs. We first examine the transient spectra of free QDs (without adsorbed MV^{2+}) under low 400 nm excitation (~27 $\mu W/cm^2$) to ensure that the signal is dominated by single exciton states. The TA spectra in the first 3 ps are shown in Figure 2C and the complete spectra up to 1 μs can be found in Figure S5. Transient signals in CdX (X = S, Se, and Te) QDs have been shown to be dominated by the transient bleach of 1S exciton absorption bands caused by the state filling of the 1S electron level.[42,43] Excitation at 400 nm creates a hot electron and hot hole above the CB and VB edges, whose relaxation to the $1S_e$ and $1S_h$ levels, respectively, leads to the continuous red-shift of the T_1 bleach and the growth of the T_0 bleach shown in Figure 2C and D. After this initial relaxation, the bleaches are long-lived, consistent with a long-lived single 1S exciton state. From the bleach recovery kinetics (Figure S5), the half-lifetime of the single exction state is determined to be ~30 ns, which is about twice as long as that in CdSe core only QDs (~15 ns) and is consistent with the reduced electron–hole wave function overlap expected in such quasi-type II QDs. In addition to the T_1 and T_0 bleach features, the TA spectra of excited QDs also show much smaller photoinduced absorption features at >610 nm, which will be further discussed later.

The TA spectra of free CdSe/CdS QDs and CdSe/CdS–MV^{2+} complexes at 5 ps are compared in Figure 3A and the corresponding kinetics at T_0, T_1 and 630 nm in the first 5 ps are compared in Figure 3B. These spectra were recorded under the same single exciton excitation conditions and the comparison of TA spectra from 100 fs to 1 μs can be found in SI5. In QD–MV^{2+} complexes, the adsorption of MV^{2+} reduces the exciton lifetime, as indicated by the complete quenching of QD emission (data not shown) and ultrafast recovery of the exciton bleaches in the transient absorption spectra. The bleaches at the T_1 and T_0 bands show much smaller initial amplitudes and nearly complete recovery in the first 5 ps compared to free QDs, in which negligible recovery was observed (Figure 3B & C), suggesting an ultrafast (hot) electron transfer from the QD to MV^{2+}. Concomitant with the QD exciton bleach recovery, derivative-like features of the exciton bands and a positive absorption band centered at ~610 nm are formed (Figure 3D). The latter feature matches well with the absorption spectrum of MV^+ radicals (Figure 3A inset), confirming the ultrafast electron transfer from CdSe/CdS QDs to MV^{2+} molecules. Furthermore, the TA spectra of the charge separated state in CdSe/CdS–benzoquinone (BQ) complexes (Figure S6) show only the exciton derivative feature and lack the band at 610 nm, consistent with the assignment of this band to $MV^{+\bullet}$. The derivative-like feature can be assigned to the Stark-effect induced exciton peak shift in the charge separated state (QD^+–$MV^{+\bullet}$) similar to those observed in the charge separated states of core/shell (CdTe/CdSe and CdSe/ZnS) QD-anthraquinone complexes.[18,19] Similar TA features are observed in CdSe–MV^{2+}(Figure S7) and CdS–MV^{2+}(Figure S8), in which the Stark-effect features are well separated from the $MV^{+\bullet}$ radical absorption band. As shown in Figures S5B and S9, after the initial formation, these Stark-effect and $MV^{+\bullet}$ radical features decay on the ns to μs time scale due to the charge recombination process. Assuming that the adsorption of MV^{2+} does not create other unobserved exciton decay pathways, the above spectral evidence (complete and ultrafast exciton bleach recovery and ultrafast formation of charge separated state) suggests that in CdSe/CdS–MV^{2+} complexes, the single exciton state in QDs decays by ultrafast electron transfer to MV^{2+} with 100% quantum yield. The growth and decay of the MV^+ radical signal at 630 nm can be fitted by multiple-exponential and stretched exponential functions, respectively (SI5). From the fit, we determine a half-life time of 0.18 ± 0.02 ps and 425 ± 20 ns for the charge separation and charge recombination processes, respectively.

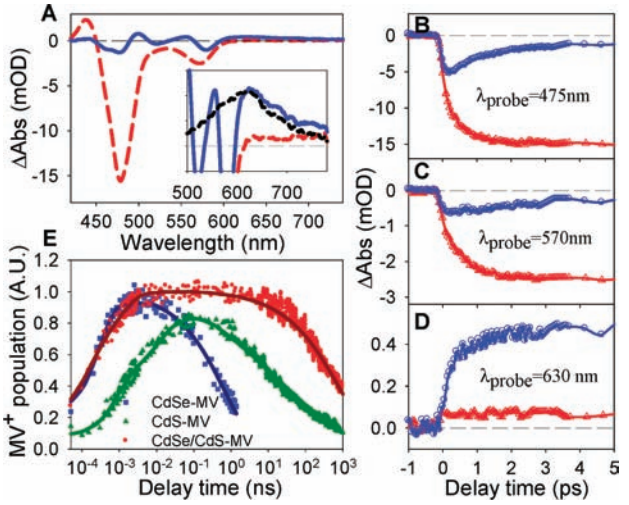

Figure 3. (A) TA spectra of free CdSe/CdS QDs (red dashed line) and CdSe/CdS–MV^{2+} complexes (blue solid line) at 5 ps after 400 nm excitation under single exciton conditions (~27 $\mu W/cm^2$). (Inset) An expanded view of the spectra at 500–750 nm and a comparison with MV^+ radical spectrum (dashed black line), showing photogenerated MV^+ radicals in the QD–MV^{2+} complexes. (B–D) Comparison of TA kinetics probed at (B) 475 nm (T_1), (C) 570 nm (T_0), and (D) 630 nm (MV^+ radical) in free CdSe/CdS QDs (red circles) and CdSe/CdS–MV^{2+} complexes (blue triangles). (E) Comparison of normalized MV^+ radical formation and decay kinetics in QD–MV^{2+} complexes of CdSe (blue), CdS (green), and CdSe/CdS (red) after 400 nm excitation.

As a comparison, the charge separation and recombination kinetics in CdSe–MV^{2+} and CdS–MV^{2+} complexes were also investigated. The details of their TA spectra, kinetics and analysis can be found in SI7 and SI8. The kinetics of MV^+ radical formation measured at ~630 nm in CdSe, CdS, and CdSe/CdS QDs are compared in Figure 3E. Compared to CdSe core only QDs, CdSe/CdS core/shell quasi type II QDs maintain a similar ultrafast charge separation rate but slow down the charge recombination process by ~1000 times. This much improved charge separation property can be attributed to the electron and hole distributions in the quasi-type II material: the delocalization of the CB electron maintains a large amplitude of electron wave function at the shell surface, enabling an ultrafast electron transfer to the adsorbates, whereas the strongly core confined VB hole reduces electronic coupling strength for the charge recombination process, resulting in a much longer lived charge separated state.[19] For reasons yet to be understood, the charge separation and recombination rates in CdS–MV^{2+} complexes are both ~10 times slower than those in CdSe–MV^{2+} complexes.

dx.doi.org/10.1021/ja210312s | J. Am. Chem. Soc. 2012, 134, 4250–4257

Multi-Exciton Dyanmics in CdSe/CdS QDs. To investigate the exciton−exciton annihilation dynamics and quantify the average number of excitons generated in CdSe/CdS QDs, we recorded TA spectra in free QDs as a function of excitation intensities from ~27 to ~4250 μW/cm^2 (see SI9). A representative set of TA spectra of CdSe/CdS QDs recorded at the highest excitation intensities (4250 μW/cm^2) is shown in Figure 4A. In addition to the bleaches at T_1 and T_0 bands, the

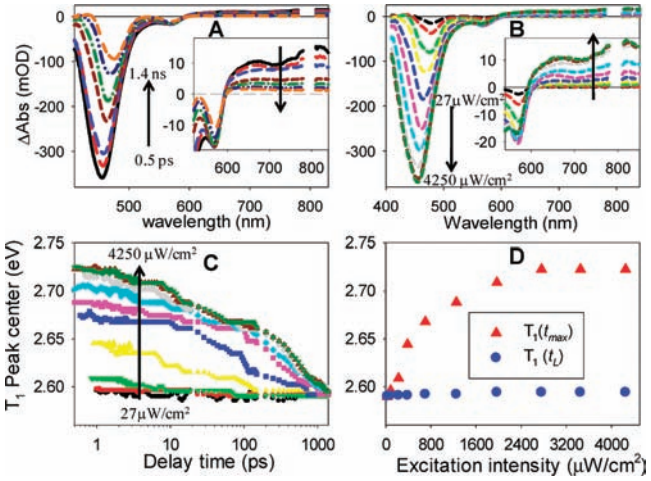

Figure 4. (A) TA spectra of CdSe/CdS QDs at 0.5 ps, 3 ps, 10 ps, 50 ps, 100 ps, 500 ps, and 1.4 ns (from bottom to top) at the highest 400 nm excitation intensity (~4250 μW/cm^2). (B) TA spectra at t_{max} (when the bleach amplitudes are largest) under different excitation intensities (from 27 to 4250 μW/cm^2). The spectra between 500 and 840 nm are expanded in the inset of (A) and (B) to more clearly show the photoinduced absorption features at >600 nm. (C) The time evolution of the T_1 bleach peak position at different excitation intensities. (D) T_1 bleach peak positions at t_{max} and t_L = 1.4 ns as a function of the excitation intensity.

transient spectra show two broad photoinduced absorption (PA) bands centered at ~640 nm (PA_1) and 825 nm (PA_2). The PA_1 feature extends into the T_0 band, but its contribution can be subtracted to reveal the kinetics of T_0 bleach only, which are shown in Figure 5A.[44] The details of the subtraction are provided in SI12. As discussed in SI6, these PA bands were shown to remain unchanged when the 1S electrons were transferred to electron acceptors and can be attributed to transitions involving the VB or trapped hole in the QD. At all excitation intensities, the amplitudes of these features (T_0, T_1, PA) initially grow and reach a maximum at t_{max} due to the initial hot electron and hole cooling process (see Figure 2C and D). The value of t_{max} ranges from 0.3 to 2 ps, becoming shorter with increasing excitation intensity, reflecting the carrier density dependent hot electron and hole relaxation time.[45]

At the lowest excitation intensity, there are negligible changes in the peak position and amplitude of these features (T_1, T_0, PA_1, and PA_2) between t_{max} and 1.4 ns, indicating that the signal is dominated by the long-lived single exciton state, as discussed previously. At higher excitation intensities, these features show fast decay components (Figure 5A and B) caused by fast exciton−exciton annihilation processes. At all excitation intensities, the transient spectra and kinetics after 1.4 ns (t_L) become identical to those at the lowest excitation intensity (see T_1 peak shift in Figure 4D and T_0 kinetics in SI10), suggesting the completion of multiexciton annihilation at this delay time and negligible sample degradation under all excitation

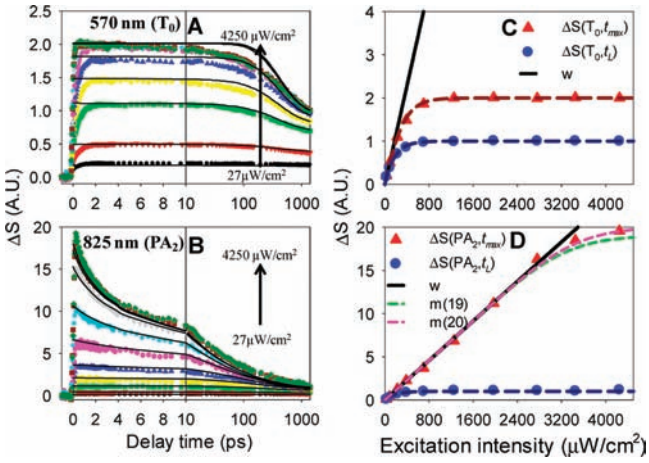

Figure 5. (Left column) Normalized transient kinetics (open symbols) at T_0 (A) and PA_2 (B) bands at different excitation intensities. The solid lines are fits to a stochastic multicarrier annihilation model described in the main text. (Right column) Normalized TA signal of T_0 (C) and PA_2 (D) at t_{max} (red circles) and t_L (blue triangles) as a function of excitation intensities. The solid and dashed lines in C and D are fits to eqs 2−4.

intensities. However, between t_{max} and 1.4 ns (t_L), these features exhibit different excitation intensity dependence in their amplitudes, peak positions and decay kinetics. For example, the T_0 bleach amplitude recovery kinetics become independent of the excitation intensity after 1250 μW/cm^2 (Figure 5A), while the PA_2 kinetics (amplitude and kinetics) and T_1 bleach (amplitude and peak shift) saturates at a higher excitation intensity (3450 μW/cm^2). As will be discussed below, these variations indicate different dependence on the number of excitons and reflect the different degeneracy of these transitions.

We first compare the TA spectra at t_{max} (Figure 4B) and the peak positions (Figure 4C) as a function of delay time for the T_1 bleach at all excitation intensities. At higher excitation intensities, the amplitude of T_1 bleach (at t_{max}) increases, its width broadens, and peak position shifts to higher energy. These features suggest the filling of more and higher energy CB electron levels at higher excitation intensities, similar to the band filling induced dynamic Burstein−Moss shift observed in many semiconductor materials.[46−48] We model the observed intensity dependence of T_1 bleach spectra by assuming a bulk like density of states for T_1 and higher energy transitions (see SI11 for details).[47] As shown in Figure S11B, the calculated spectra reproduce the blue shift, broadening and amplitude increase of the T_1 bleach band at higher excitation intensities. The qualitative agreement suggests a quasi-continuum of conduction band states in the CdSe/CdS QDs, consistent with the bulk-like UV−vis absorption features above the T_1 transition and the calculated weekly confined electron levels. We note that the initial peak position appears to no longer increase after the excitation intensity reaches 3450 μW/cm^2 (Figure 4D), suggesting the saturation of the number of excitons generated in the QDs. This peak position is lower than 3.2 eV, suggesting that not all states at the excitation and lower energies are filled. The saturation is likely a transient effect during the excitation pulse, after which, some of the hot electrons and holes relax to fill the lower lying states, shifting the bleach to lower energy.

dx.doi.org/10.1021/ja210312s | J. Am. Chem. Soc. 2012, 134, 4250−4257

To quantify the number of excitons in the QD at any given excitation intensity level, we analyze the intensity dependence of the TA signal at T_0 and PA_2 bands. Excitation at 400 nm (or 3.2 eV) creates electron and hole pairs at 1 eV above the band edge. We assume that the probability of a QD encountering n photons, $f(n)$, within the laser pulse duration is governed by the Poisson statistics: $f(n) = w^n e^{-w}/n!$.[21,42] Here w is the average number of encountered photons, which scales with the excitation pulse energy (I), i.e., $w = CI$. The scaling factor C, dependent on the absorption cross section as well as the pump and probe beam geometries and overlaps, cannot be accurately calculated. Instead, we rely on the fitting procedure to be discussed below to determine its value, which enables the determination of the average number of excitons at any given excitation intensity. The total number of excitons that can be created within the excitation pulse depends on the competition between the photon absorption and electron/hole relaxation to lower lying levels to avoid saturation. At low excitation fluence, when the absorption rate is low compared to the relaxation rate, every QD-photon encounter leads to the absorption of one photon and the generation of one exciton. At high excitation fluence, the photon encounter rate may exceed the electron/hole relaxation rate, leading to a transient saturation of the absorption process within the excitation pulse duration. We assume that there is a maximum number (N_{max}) of excitons that can be generated in each QD. After reaching N_{max}, the random encounter no longer leads to a photon absorption and exciton generation event. At early delay time ($t = t_{max}$, prior to the exciton−exciton annihilation process), the number of excitons (n) generated in a QD can be assumed to obey the Poisson distribution ($P(n,t_{max}) = f(n) = w^n e^{-w}/n!$) at $n < N_{max}$, and saturates at $n = N_{max}$, i.e., $P(N_{max},t_{max}) = 1 - \sum_{n=0}^{N_{max}-1} f(n)$. The average number of excitons in the QDs (m) is given by

$$m(N_{max}) = \sum_{n=0}^{N_{max}} P(n, t_{max})n \quad (1)$$

It predicts that $m(N_{max}) = w = CI$ when $m \ll N_{max}$ but saturates when m approaches N_{max}.

As discussed above, at $t_L = 1.4$ ns, all multiple excitons have annihilated and only single exciton states remain. Therefore, at $t_L = 1.4$ ns, the transient signal amplitudes, $\Delta A(\lambda,t_L)$, at T_0 and PA_2 bands are proportional to the number of excited QDs: $\Delta A(\lambda,t_L) = \alpha(\lambda)[1 - P(0,t_{max})]$, where $\alpha(\lambda)$ is a wavelength dependent scaling factor that is proportional to the extinction coefficients of these transitions. We define a normalized transient signal

$$\begin{aligned}\Delta S(\lambda, t_L) &= \Delta A(\lambda, t_L)/\alpha(\lambda) \\ &= 1 - P(0, t_{max}) \\ &= 1 - e^{-w}\end{aligned} \quad (2)$$

These normalized transient absorption signals represent the probability of finding excited QDs in the ensemble. At high excitation intensities, when all QDs are excited, $\Delta S(\lambda,t_L)$ approaches one, from which we can determine the normalization factor $\alpha(\lambda)$. The transient signals at other delay times are also normalized by the same scaling factor to obtain normalized transient signals, $\Delta S(\lambda,t) = \Delta A(\lambda,t)/\alpha(\lambda)$, which are shown in the kinetics traces in Figure 5A and B.

The transient bleach signal at T_0 band is determined by the state filling of the 1S electron level. Because of the 2 fold spin degeneracy of this level, we assume that the T_0 bleach amplitude in QDs with multiple ($n \geq 2$) excitons is twice as large as that with a single exciton. Therefore, the initial normalized transient bleach signal at t_{max} is given by

$$\begin{aligned}\Delta S(T_0, t_{max}) &= P(1, t_{max}) + 2[1 - P(0, t_{max}) \\ &\quad - P(1, t_{max})] \\ &= 2 - (2 + w)e^{-w}\end{aligned} \quad (3)$$

It predicts that at $w \gg 1$, when all QDs have two or more excitons, $\Delta S(T_0,t_{max})$ approaches 2.

The transient absorption signal PA_2 appears to increase linearly with excitation power (or the average number of excitons). The corresponding normalized transient signal at t_{max} is

$$\Delta S(PA_2, t_{max}) = \sum_n nP(n, t_{max}) = m \quad (4)$$

The normalized transient signals,$\Delta S(\lambda,t_L)$ and $\Delta S(\lambda,t_{max})$, at T_0 and PA_2 bands are plotted as a function of excitation intensities in Figure 5C and D. These data can be fit by eqs 2−4 with the scaling factor C (=I/w) and N_{max} as the only fitting parameters. These data are well fit by this model, from which the average number of excitons (m) at all excitation powers can be obtained. The normalized transient absorption signal $\Delta S(PA_2,t_{max})$ (or m) increases linearly with the excitation intensity until $m > 16$. At higher excitation intensity, the signal saturates, deviating from a linear dependence on the excitation intensity. Similar saturation behavior was observed in the T_1 bleach position (Figure 4D) indicating that there is an upper limit to the number of excitons in the QD. The saturation behavior can be best fit with $N_{max} = 20$. Our result suggests that these QDs can accommodate a maximum of 20 excitons per QD at 400 nm excitation. At the highest excitation intensity (4250 $\mu W/cm^2$) used in this study, the average number of excitons per QD reaches 19 in our sample.

The decay of the normalized transient signals at T_0 and PA_2 from the initial distribution of multiple excitons states, $\Delta S(\lambda,t_{max})$, to the final single exciton states,$\Delta S(\lambda,t_L)$, is governed by the multiple exciton decay dynamics. The kinetics at T_0 and PA_2 are different due to their different dependence on the number of excitons as discussed above. The normalized transient signals at T_0 and PA_2 transition at delay time t are given by

$$\Delta S(T_0, t) = P(1, t) + 2[1 - P(0, t) - P(1, t)] \quad (5)$$

$$\Delta S(PA_2, t) = \sum_n nP(n, t) \quad (6)$$

where $P(n,t)$ is the probability of finding QDs with n excitons at time t. Assuming that n-exciton state can only decay sequentially (to $n - 1$ exciton state) by auger recombination (with time constant τ_n), the time-dependent distribution of multiexciton states in QDs is described by a set of coupled rate equations[26,49,50]

$$\frac{dP(n, t)}{dt} = \frac{P(n + 1, t)}{\tau_{n+1}} - \frac{P(n, t)}{\tau_n} \quad (7)$$

The single exciton state lifetime is assumed to be 30 ns. Because it is ≫1.4 ns, it does not significantly influence the kinetics shown in Figure 5A and B. The initial exciton distribution, $P(n,t_{max})$, at a certain excitation power has been

obtained from fitting the early time and longer time transient signal amplitudes shown in Figure 5C and D. The Auger recombination time of n-exciton states have been reported to obey quadratic ($\tau_n^{-1} \propto n^2$), cubic ($\tau_n^{-1} \propto n^3$) or statistical ($\tau_n^{-1} \propto n^2(n-1)$) scaling laws, depending on the materials and size.[26,28] From the calculated $P(n,t)$, fits to the normalized kinetics at T_0 and PA_2 can be obtained using eqs 5 and 6, respectively. As shown in Figure 5A and B, the kinetics of both T_0 and PA_2 at most excitation intensities can be well fit by this model with the biexciton lifetime (τ_2) as the only fitting parameter. The statistical scaling law yields the best fit, from which, we obtain the biexction lifetime and deduce lifetimes of all other higher order-exciton states ($\tau_2 \approx 440$ ps, $\tau_{19} \approx 270$ fs), which are listed in Table S5. As a comparison, the biexciton lifetime in the CdSe core only QD (1.2 nm radius, without the CdS shell) is ~6 ps,[26] or 80 times shorter. The biexciton lifetime in a CdSe QDs of the same size (3.4 nm radius) can be estimated to be ~130 ps from a volume scaling law,[25] which is about 4 times shorter. The prolonged biexciton lifetime in CdSe/CdS QDs can be attributed to reduced electron–hole wave function overlap in this quasi-type II structure[37] and possibly to alloy formation at the core/shell interface.[39] The fits deviate substantially from the experimental data at high exciton number ($m > 12$) per QDs, the reason for which is yet to be understood. It may suggest the failure the statistical scaling law, which assumes that all electrons and holes are equal in the Auger recombination process, and/or the presence of other recombination pathways at high carrier densities.

Multi-Exciton Charge Separation and Recombination. We conducted TA measurement on QD–MV^{2+} complexes as a function of excitation intensities under the same conditions as those for free QDs. Because MV^{2+} molecules do not absorb at 400 nm, the average number of excitons generated in the QD–MV^{2+} complex at a given excitation intensity should be the same as in free QDs and have been quantified above. By measuring the average number of MV^+ radicals generated under these conditions, the average number of dissociated excitons can be determined. The complete set of transient spectra at different excitation intensities are shown in SI9. It shows the formation of MV^+ radical absorption band at 630 nm and the corresponding recovery of the QD exciton bleach at early delay times. The TA spectra at ~8–10 ps, when the amplitude of MV^+ radical absorption band reaches the maximum, are compared in Figure 6A for all excitation intensities. The comparison shows that the amplitude of MV^+ radical absorption increases with excitation intensity until it saturates at 3450 μW/cm^2 when the average number of excitons per QD also saturates.

From the amplitude of MV^+ radical TA absorption signal $\Delta A(MV^+)$ we calculate the average number of radicals per QD (S_{MV^+}): $S_{MV^+} = \Delta A(MV^+)/\alpha(MV^+)$. Here $\alpha(MV^+)$ is a scaling factor that depends on the extinction coefficients MV^+ radical and QD concentration. As discussed above, at the lowest excitation intensity (when multiple excitons are negligible), every exciton dissociates by electron transfer to MV^{2+} to generate a MV^+ radical, i.e., $S_{MV^+} = m$. Therefore, we scaled the MV^+ signal at 630 nm (at 8–10 ps) by a factor $\alpha(MV^+)$ such that it equals to m at this low excitation intensity. The same scaling factor is applied to all the measured MV^+ signal amplitudes (at 8–10 ps) at higher excitation intensities. Thus, the normalized MV^+ signal represents the average number of MV^+ radicals (or dissociated excitons) per QD. We note that the TA signal at 630 nm contains a small portion (14–18%) of

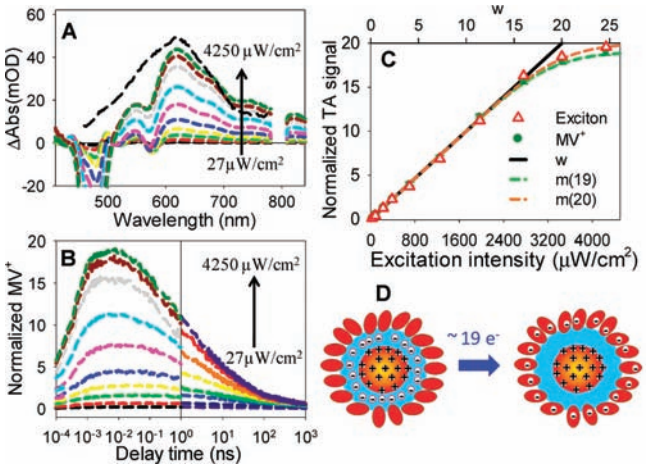

Figure 6. (A) Average TA spectra of QD–MV^{2+} complexes at 8–10 ps (when the MV^+ radical signal has reached maximum) at indicated excitation intensities. (B) Kinetics of normalized MV^+ radical TA signal at 630 nm in QD–MV^{2+} complexes. The normalized MV^+ radical signal represents the average number of MV^+ radicals per QD (see the main text for details). (C) Normalized MV^+ radical signal (at 8–10 ps) in QD–MV^{2+} complexes as a function of excitation intensities. (D) Schematic depiction of ultrafast transfer of 19 electrons from CdSe/CdS QDs to adsorbed MV^{2+} molecules.

QD PA signal, which has been determined in the free QD samples and subtracted from the total signal in QD–MV^{2+} complexes to obtain the MV^+ radical signal (see Figure S13). The normalized MV^+ radical signals at 8–10 ps as a function of excitation intensity are plotted in Figure 6C (dark green dot). It shows that the average number of MV^+ radicals per QD (S_{MV^+}) closely follows the average number of excitons generated (m) in the free QD, suggesting that all excitons generated in the QDs under 400 nm illumination can be dissociated by electron transfer to MV^{2+} to produce MV^+ radicals with nearly 100% quantum yield. At the highest excitation intensity (4250 μW/cm^2), on average, 19 excitons were generated and dissociated from each QD to produce 19.1 ± 0.5 MV^+ radicals. The error bar reflects the standard deviation of two measurements.

To follow the fate of the multiple-charge separated state, we have plotted the normalized MV^+ radical signals (i.e., the average number of MV^+ radicals per QD) as a function of time from femtoseconds to microseconds in Figure 6B. The data before and after 1.4 ns were acquired at different instruments with different excitation intensities. The kinetics traces acquired at the highest excitation intensities connects smoothly because the average number of dissociated excitons (and hence MV^+ radicals) saturates to the same value in the QDs. Below saturation, these kinetics do not connect well because different excitation intensities. It is interesting to note that the exciton dissociation rates remain ultrafast even when 19 excitons were dissociated. The enhanced electron–electron repulsion and weakened electron–hole attraction in this kind of quasi-type II structures[37,41] may account for this ultrafast multielectron transfer rates. With increasing number of dissociated excitons, the MV^+ radical kinetics shows a faster decay, suggesting a faster charge recombination process (of the holes in the QDs and electrons in MV^+ radicals), which is consistent with bimolecular nature of this process. Nevertheless, the half-life times of charge separated states with two and nineteen dissociated excitons in one QD are ~80 and ~2.3 ns,

dx.doi.org/10.1021/ja210312s | J. Am. Chem. Soc. 2012, 134, 4250–4257

respectively, in this core/shell structure, suggesting the possibility of driving multielectron catalytic reactions.

CONCLUSION

Semiconductor nanomaterials can continue to absorb photons at excited or charged states, offering the possibility to deliver multiple electrons/holes needed in solar-to-fuel conversion devices. The quantum confinement of electron and hole in semiconductor nanocrystals enhances ultrafast charge separation rate, but it also enhances the rates of charge recombination and exciton−exciton annihilation (by Auger recombination), hindering the efficient extraction of multiple carriers. In nanoheterostructures with type II or quasi type II band alignment, it is possible to tailor the distributions of electron and hole wave functions to selectively control these rates. Using CdSe/CdS quasi-type II core shell QDs, we demonstrate that ultrafast charge separation, ultraslow charge recombination and slow exciton Auger annihilation can be simultaneously achieved. With adsorbed methylviologen molecules as model electron acceptors, nineteen excitons per QD can be dissociated with unity yield by electron transfer to the adsorbed MV^{2+} and the lifetime of the multiple-charge separated state is lengthened considerably compared to core only QDs.

Our study demonstrates that type II nanoheterostructures can be used as potential light harvesting and charge separation components in artificial photosynthetic systems to enhance multiple exciton dissociation efficiencies. For practical applications, it is desirable to remove the valence band holes efficiently by external circuit or other electron sources, which can be facilitated in linear or branched type II heterostructures where both carriers are exposed to charge collection network.[51,52] Furthermore, efficient exciton dissociation would need to be coupled with schemes of generating multiple excitons. Direct MEG by one high energy photon has been reported in type II materials with threshold energy below that for each constituent material.[53] Alternatively, methods to enhance light harvesting rates of nanoheterostructures by plasmonic enhancement[54] and by building large QD-antenna complexes should also be explored.

ASSOCIATED CONTENT

Supporting Information

Additional text, figures, and tables showing experimental methods, effective mass calculation, excitation wavelength dependence, TA spectra of QD and QD-MV^{2+} at all excitation intensities from fs to μs, PA signal assignment, T_1 dynamic Burstein−Moss shift modeling, and fitting parameters. This material is available free of charge via the Internet at http://pubs.acs.org.

AUTHOR INFORMATION

Corresponding Author

tlian@emory.edu

Notes

The authors declare no competing financial interest.

ACKNOWLEDGMENTS

The authors gratefully acknowledge the support from the National Science Foundation (CHE-0848556)

REFERENCES

(1) Lewis, N. S.; Nocera, D. G. *Proc. Natl. Acad. Sci.* **2006**, *103*, 15729.
(2) Gratzel, M. *Nature* **2001**, *414*, 338.
(3) Esswein, A. J.; Nocera, D. G. *Chem. Rev.* **2007**, *107*, 4022.
(4) Walter, M. G.; Warren, E. L.; McKone, J. R.; Boettcher, S. W.; Mi, Q.; Santori, E. A.; Lewis, N. S. *Chem. Rev.* **2010**, *110*, 6446.
(5) Hill, R.; Bendall, F. A. Y. *Nature* **1960**, *186*, 136.
(6) Mitchell, P. *Biol. Rev. Cambridge Philos. Soc.* **1966**, *41*, 445.
(7) Bach, U.; Lupo, D.; Comte, P.; Moser, J. E.; Weissortel, F.; Salbeck, J.; Spreitzer, H.; Gratzel, M. *Nature* **1998**, *395*, 583.
(8) Kamat, P. V.; Tvrdy, K.; Baker, D. R.; Radich, J. G. *Chem. Rev.* **2010**, *110*, 6664.
(9) Gur, I.; Fromer, N. A.; Geier, M. L.; Alivisatos, A. P. *Science* **2005**, *310*, 462.
(10) Brown, K. A.; Dayal, S.; Ai, X.; Rumbles, G.; King, P. W. *J. Am. Chem. Soc.* **2010**, *132*, 9672.
(11) Sambur, J. B.; Novet, T.; Parkinson, B. A. *Science* **2010**, *330*, 63.
(12) Nair, G.; Chang, L.-Y.; Geyer, S. M.; Bawendi, M. G. *Nano Lett.* **2011**, *11*, 2145.
(13) Nozik, A. J. *Nano Lett.* **2010**, *10*, 2735.
(14) Beard, M. C. *J. Phys. Chem. Let.* **2011**, *2*, 1282.
(15) McGuire, J. A.; Joo, J.; Pietryga, J. M.; Schaller, R. D.; Klimov, V. I. *Acc. Chem. Res.* **2008**, *41*, 1810.
(16) Pijpers, J. J. H.; Ulbricht, R.; Tielrooij, K. J.; Osherov, A.; Golan, Y.; Delerue, C.; Allan, G.; Bonn, M. *Nat. Phys.* **2009**, *5*, 811.
(17) Landsberg, P. T. *Recombination in semiconductors*; Cambridge University Press: New York, 2003.
(18) Zhu, H.; Song, N.; Lian, T. *J. Am. Chem. Soc.* **2010**, *132*, 15038.
(19) Zhu, H.; Song, N.; Lian, T. *J. Am. Chem. Soc.* **2011**, *133*, 8762.
(20) Tisdale, W. A.; Williams, K. J.; Timp, B. A.; Norris, D. J.; Aydil, E. S.; Zhu, X.-Y. *Science* **2010**, *328*, 1543.
(21) Huang, J.; Huang, Z.; Yang, Y.; Zhu, H.; Lian, T. *J. Am. Chem. Soc.* **2010**, *132*, 4858.
(22) Matylitsky, V. V.; Dworak, L.; Breus, V. V.; Basche, T.; Wachtveitl, J. *J. Am. Chem. Soc.* **2009**, *131*, 2424.
(23) Dworak, L.; Matylitsky, V. V.; Breus, V. V.; Braun, M.; Basché, T.; Wachtveitl, J. *J. Phys. Chem. C* **2011**, *115*, 3949.
(24) Morris-Cohen, A. J.; Frederick, M. T.; Cass, L. C.; Weiss, E. A. *J. Am. Chem. Soc.* **2011**, *133*, 10146.
(25) Robel, I.; aacute; Gresback, R.; Kortshagen, U.; Schaller, R. D.; Klimov, V. I. *Phys. Rev. Lett.* **2009**, *102*, 177404.
(26) Klimov, V. I.; Mikhailovsky, A. A.; McBranch, D. W.; Leatherdale, C. A.; Bawendi, M. G. *Science* **2000**, *287*, 1011.
(27) Efros, A. L.; Kharchenko, V. A.; Rosen, M. *Solid State Commun.* **1995**, *93*, 281.
(28) Klimov, V. I.; McGuire, J. A.; Schaller, R. D.; Rupasov, V. I. *Phys. Rev. B* **2008**, *77*, 195324.
(29) Tisdale, W. A.; Zhu, X.-Y. *Proc. Natl. Acad. Sci.* **2011**, *108*, 965.
(30) Cragg, G. E.; Efros, A. L. *Nano Lett.* **2010**, *10*, 313.
(31) Zavelani-Rossi, M.; Lupo, M. G.; Tassone, F.; Manna, L.; Lanzani, G. *Nano Lett.* **2010**, *10*, 3142.
(32) Müller, J.; Lupton, J. M.; Lagoudakis, P. G.; Schindler, F.; Koeppe, R.; Rogach, A. L.; Feldmann, J.; Talapin, D. V.; Weller, H. *Nano Lett.* **2005**, *5*, 2044.
(33) Borys, N. J.; Walter, M. J.; Huang, J.; Talapin, D. V.; Lupton, J. M. *Science* **2010**, *330*, 1371.
(34) Pandey, A.; Guyot-Sionnest, P. *Science* **2008**, *322*, 929.
(35) Zhu, H.; Yang, Y.; Song, N.; Rodríguez-Cordoba, W.; Lian, T. *Proc. SPIE* **2011**, *8098*, 809802.
(36) Brovelli, S.; Schaller, R. D.; Crooker, S. A.; García-Santamaría, F.; Chen, Y.; Viswanatha, R.; Hollingsworth, J. A.; Htoon, H.; Klimov, V. I. *Nat. Commun.* **2011**, *2*, 280.
(37) Oron, D.; Kazes, M.; Banin, U. *Phys. Rev. B* **2007**, *75*, 035330.
(38) García-Santamaría, F.; Chen, Y.; Vela, J.; Schaller, R. D.; Hollingsworth, J. A.; Klimov, V. I. *Nano Lett.* **2009**, *9*, 3482.
(39) García-Santamaría, F.; Brovelli, S.; Viswanatha, R.; Hollingsworth, J. A.; Htoon, H.; Crooker, S. A.; Klimov, V. I. *Nano Lett.* **2011**, *11*, 687.

(40) Li, J. J.; Wang, Y. A.; Guo, W. Z.; Keay, J. C.; Mishima, T. D.; Johnson, M. B.; Peng, X. G. *J. Am. Chem. Soc.* **2003**, *125*, 12567.
(41) Sitt, A.; Sala, F. D.; Menagen, G.; Banin, U. *Nano Lett.* **2009**, *9*, 3470.
(42) Klimov, V. I. *J. Phys. Chem. B* **2000**, *104*, 6112.
(43) Klimov, V. I. *Annu. Rev. Phys. Chem.* **2007**, *58*, 635.
(44) Lupo, M. G.; Della Sala, F.; Carbone, L.; Zavelani-Rossi, M.; Fiore, A.; Lüer, L.; Polli, D.; Cingolani, R.; Manna, L.; Lanzani, G. *Nano Lett.* **2008**, *8*, 4582.
(45) Tsen, K. T. *Ultrafast physical processes in semiconductors*; Academic Press: New York, 2001; Vol. *67*.
(46) Liu, C. Y.; Bard, A. J. *J. Phys. Chem.* **1989**, *93*, 3232.
(47) Puthussery, J.; Lan, A.; Kosel, T. H.; Kuno, M. *ACS Nano* **2008**, *2*, 357.
(48) Kamat, P. V.; Dimitrijevic, N. M.; Nozik, A. J. *J. Phys. Chem.* **1989**, *93*, 2873.
(49) Hilczer, M.; Tachiya, M. *J. Phys. Chem. C* **2009**, *113*, 18451.
(50) Barzykin, A. V.; Tachiya, M. *J. Phys.: Condens. Matter* **2007**, *19*, 065105.
(51) Milliron, D. J.; Hughes, S. M.; Cui, Y.; Manna, L.; Li, J. B.; Wang, L. W.; Alivisatos, A. P. *Nature* **2004**, *430*, 190.
(52) Talapin, D. V.; Nelson, J. H.; Shevchenko, E. V.; Aloni, S.; Sadtler, B.; Alivisatos, A. P. *Nano Lett.* **2007**, *7*, 2951.
(53) Gachet, D.; Avidan, A.; Pinkas, I.; Oron, D. *Nano Lett.* **2009**, *10*, 164.
(54) Atwater, H. A.; Polman, A. *Nat. Mater.* **2010**, *9*, 205.